Parameter Stability Region Analysis of Islanded Microgrid Based on Bifurcation Theory

Shuai, Zhikang; Peng, Yelun; Liu, Xuan; Li, Zuyi; Guerrero, J. M.; Shen, John

Published in:
IEEE Transactions on Smart Grid

DOI (link to publication from Publisher):
10.1109/TSG.2019.2907600

Publication date:
2019

Document Version
Accepted author manuscript, peer reviewed version

This article has been accepted for publication in a future issue of this journal, but has not been fully edited. Content may change prior to final publication. Citation information: DOI 10.1109/TSG.2019.2907600, IEEE Transactions on Smart Grid

Parameter Stability Region Analysis of Islanded Microgrid Based on Bifurcation Theory

Zhikang Shuai, *Senior Member, IEEE*, Yelun Peng, Xuan Liu, *Member, IEEE*, Zuyi Li, *Senior Member, IEEE*, Josep M. Guerrero, *Fellow, IEEE* and John Shen, *Fellow, IEEE*

***Abstract*-- This paper studies the parameter stability region of droop-controlled AC microgrid (MG) with static ZIP (constant impedance, constant current, constant power) load and dynamic induction motor (IM) load using bifurcation theory. First, the dynamic model of the MG with ZIP and IM loads is developed. Next, bifurcation analysis is used to predict the bifurcation boundaries where microgrid becomes unstable. Saddle node and hopf bifurcation are detected in the studied system when parameters change. The stability region in parameters space is bounded by bifurcation boundaries. To improve the computing efficiency for predicting the stable region of parameters, the reduced-order models of MGs are developed based on singular perturbation method. Finally, numerical simulations and experiment are used to verify the analysis result and the effectiveness of the proposed strategy.**

***Index Terms*-- Islanded microgrid, parameter stability region, bifurcation theory, reduced-order model, singular perturbation method.**

I. Introduction

The Microgrids (MGs) that serve as individual controllable systems can integrate distributed generators (DGs) and supply power to local loads with or without external power systems [1]. The low-inertia and limited capabilities of inverter make MG vulnerable to instability when subject to disturbances [2-4]. In practical case, multiple types of load are considered in MG system, such as resistance load, constant power load and induction motor (IM) load. To achieve stable operation, the parameter stability region of MG with multitype loads need to be predicted [5].

Small-signal analysis has been widely used to investigate the stability of the linearized system under a set of specific parameter configuration [6-9]. However, when system parameters change, the equilibrium is accordingly changed and deviates from the predefined linearization point [10-14]. To plot the stability constraint of parameters, the linearization and eigenvalue calculation are performed iteratively, which is labor-consuming and inefficient.

The bifurcation analysis has been proposed to predict the parameter stability boundary of nonlinear system. Bifurcation occurs when a small continuously change of parameter values causes a sudden change in system behavior [14]. Compared with the small-signal analysis that analyzes the perturbation of a fixed equilibrium, the bifurcation analysis can perform parametric stability analysis that traces equilibrium solutions as the parameters change [15-16]. In [17-19], the bifurcation theory was used to predict the parameter stability region of MG. However, only RL load [17-18] and rectifier served as a constant-power load [19] are considered. ZIP (constant impedance, constant current, constant power) load is widely used to describe a practical static load, which is rarely considered in current MG models. In [20], the progressive increment of IM load was given by placing identical IMs in parallel. However, the MG model is changed with the increase of connected IMs, which prevents the continuous tracing of the equilibrium manifold. So far, the bifurcation analysis for MG with ZIP and IM load have not been discussed.

Another problem of the stability-region analysis is the high dimension of MG model, which results in a huge computation burden. Singular perturbation method has been proposed to reduce the model order by eliminating the fast dynamics [21-24]. However, the coupling of dynamics makes the reduced model inaccurate for predicting different boundary. In [25-27], the reduced model for predicting the stability region of active-power droop gain are proposed. However, these model present errors for predicting the stability boundary of other parameters, such as reactive power droop gain.

This paper extends the application of bifurcation theory to analyze the parameter stability region of the MG with static ZIP load and dynamic IM load. The main contributions of this paper can be summarized as follows:

(1) The equivalent model of static ZIP loads and dynamic IM loads have been developed, respectively, for the continuous tracing of the load increasing in MG model.

(2) The parameter stability region analysis based on bifurcation theory is performed for the MG with ZIP load and IM load. Bifurcation phenomena of MG with parameters change are observed. The stability boundaries of MG in terms of the key control parameters and load are investigated in detail.

(3) The reduced models for predicting different bifurcation boundaries are developed. The reduced model for predicting a specific bifurcation phenomenon preserves the states variables that has major influence on the corresponding bifurcation.

The rest of this paper is organized in the following way:

Manuscript received July 19, 2018; revised, September 03, 2018 and December 12, 2018; accepted March 22, 2019. This work was supported by the National Natural Science Foundation of China under Grant 51622702, and National Key R&D Program of China under Grant 2017YFB1200900. (*Corresponding author: Zhikang Shuai.*)

Z. Shuai, Y. Peng, and X. Liu are with the College of Electrical and Information Engineering, Hunan University, Changsha 410082, China (e-mail: zhikangshuai@hotmail.com; pengyelun@163.com; yongli@hnu.edu.cn).

Z. Li and Z. J. Shen are with the Department of Electrical and Computer Engineering, Illinois Institute of Technology, Chicago, IL 60616 USA (e-mail: lizu@iit.edu; zjohnshen@gmail.com).

Josep M. Guerrero is with the Department of Energy Technology, Aalborg University, 9220 Aalborg, Denmark (e-mail: joz@et.aau.dk).

.

This article has been accepted for publication in a future issue of this journal, but has not been fully edited. Content may change prior to final publication. Citation information: DOI 10.1109/TSG.2019.2907600, IEEE Transactions on Smart Grid

Section II describes the dynamic model of MGs with ZIP and IM loads. In Section III, bifurcation method is proposed to predict the parameter stability region of MG. In Section IV, the reduced models for stability region analysis are proposed. In Section V, simulation and experiment results are given to verify the bifurcation analysis results. Section VI concludes this paper.

II. Modeling of the Microgrid with ZIP and IM Load

This section provides the microgrid model with ZIP and IM load. The MG model consists of the droop-controlled DG, dynamic IM load, static ZIP load, and network. The equivalent model of IM and ZIP load will be presented in detail.

A. Model of the Droop-Controlled DG

The block diagram of a droop-controlled DG is depicted in Fig. 1 [6]. The control system is composed of droop controller for power sharing and inner control loops for voltage and current control. The droop controller mimics the active-power and reactive-power droop characteristics of synchronous generator. The droop controller compares the filtered active power P and reactive power Q to the command values, and outputs the frequency command ω and voltage reference u_o^{ref}. The inner-control loop is designed under the dq synchronous reference frame for voltage tracking with zero steady-state error. The PI controller for voltage control compares the u_o^{ref} and 0 to the capacitor voltage u_{od} and u_{oq}, respectively, and outputs the current reference i_{ld}^{ref} and i_{lq}^{ref}. The obtained current references are sent to the current controller where the measured current i_{ld} and i_{lq} are compared to i_{ld}^{ref} and i_{lq}^{ref}, respectively. Command voltage u_{id}, u_{iq} are given via the current controller and transformed into abc reference frame for PWM generation.

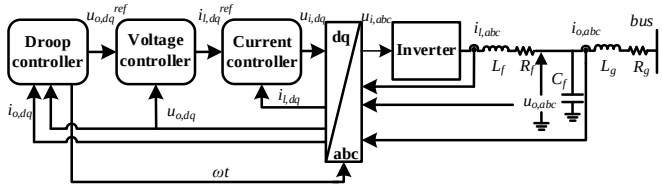

Fig. 1. Block diagram of droop-controlled inverter.

The mathematical model of droop-controlled inverter in [6] is adopted in this paper. The droop-controlled DG incorporates 12 states to describe its dynamic behavior, whose state variables are written as follows:

$$x_{DG}=[\theta, P, Q, u_{od}, u_{oq}, i_{ld}, i_{lq}, i_{od}, i_{oq}, \varphi_d, \varphi_q, \gamma_d, \gamma_q]$$

where $\varphi_d, \varphi_q, \gamma_d, \gamma_q$ are the dynamic states of PI controllers.

B. Model of the Induction Motor Load

Squirrel cage IM is selected in this work as a kind of typical IM load. The electromagnetic transients of rotor and stator sides are both considered. The flux equations of IM can be written as:

$$\psi_{sD} = L_s i_{sD} + L_m i_{rD}, \psi_{sQ} = L_s i_{sQ} + L_m i_{rQ}, \quad (1)$$

$$\psi_{rQ} = L_r i_{rD} + L_m i_{sD}, \psi_{rQ} = L_r i_{rQ} + L_m i_{sQ}, \quad (2)$$

where L_m is the linkage inductance, L_s and L_r are the stator inductance and rotor inductance, respectively. The voltage equations of IM are written as:

$$u_{sD} = R_s i_{sD} + \dot{\psi}_{sD} - \omega_{com}\psi_{sQ}, \quad (3)$$

$$u_{sQ} = R_s i_{sQ} + \dot{\psi}_{sQ} + \omega_{com}\psi_{sD}, \quad (4)$$

$$0 = R_r i_{rD} + \dot{\psi}_{rD} - (\omega_{com} - \omega_r)\psi_{rQ}, \quad (5)$$

$$0 = R_r i_{rQ} + \dot{\psi}_{rQ} + (\omega_{com} - \omega_r)\psi_{rD}, \quad (6)$$

where R_s and R_r are the stator resistance and rotor resistance, respectively. Substituting (1-2) into (3-6) and the cooperating rotor motion equation, the dynamic model of the IM can be written as:

$$\dot{\omega}_r = \frac{n_p^2 L_m}{J L_r}(i_{sQ}\psi_{rD} - i_{sD}\psi_{rQ}) - \frac{n_p}{J}T_l, \quad (7)$$

$$\dot{\psi}_{rD} = -\frac{1}{T_r}\psi_{rD} + (\omega_{com} - \omega)\psi_{rQ} + \frac{L_m}{T_r}i_{sD}, \quad (8)$$

$$\dot{\psi}_{rQ} = -\frac{1}{T_r}\psi_{rQ} - (\omega_{com} - \omega)\psi_{rD} + \frac{L_m}{T_r}i_{sQ}, \quad (9)$$

$$\dot{i}_{sD} = \frac{L_m}{\sigma L_s L_r T_r}\psi_{rD} + \frac{L_m}{\sigma L_s L_r}\omega_{com}\psi_{rQ} - \frac{R_s L_r^2 + R_r L_m^2}{\sigma L_s L_r^2} i_{sD} + \omega_{com} i_{sQ} + \frac{u_{bD}}{\sigma L_s} \quad (10)$$

$$\dot{i}_{sQ} = \frac{L_m}{\sigma L_s L_r T_r}\psi_{rQ} - \frac{L_m}{\sigma L_s L_r}\omega_{com}\psi_{rD} - \frac{R_s L_r^2 + R_r L_m^2}{\sigma L_s L_r^2} i_{sQ} - \omega_{com} i_{sD} + \frac{u_{bQ}}{\sigma L_s} \quad (11)$$

where J is the rotor inertia coefficient. $\sigma = 1 - \frac{L_m^2}{L_s L_r}$ denotes the leakage factor and $T_r = L_r/R_r$ represents the rotor electromagnetic time constant. The load torque can be described by the following nominal as:

$$T_l = T_0 + T_1\omega + T_2\omega^2. \quad (12)$$

The incremental IM load at a given bus can be obtained by placing identical IMs in parallel. However, to track the increment of IM loads, the number of integrated IMs increases at the given bus, which will change the structure and increase the size of MG model. On the other hand, the paralleled IMs can be presented as a single-unit equivalent IM based on the dynamic equivalent method. By doing so, the continuous load increment can be presented as the parameters change of the equivalent IM.

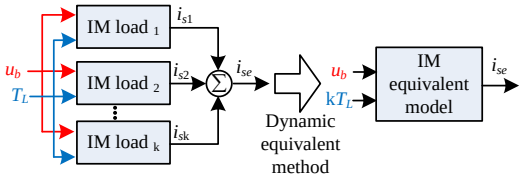

Fig.2. Bock diagram of paralleled IM loads and their equivalent model.

Fig.2 presents the signal flow of an IM model, the input signals of IM loads are bus voltage u_b and load torque T_L, stator current i_s is the output signal. To provide the same dynamic behavior with the original paralleled IMs, the dynamic equivalent model of IMs must meet the following requirements:

1) The voltage and current on the connected bus do not change.

2) The active and reactive power assumption of equivalent IMs must be equal to the sum of all the power assumption at the connected bus of paralleled IMs.

3) The electromagnetic time constant of the equivalent IM equal to that of the paralleled IMs.

According to the first condition, the stator current and bus voltage of the equivalent IM should satisfy

$$i_{sDe} = \sum i_{sD} = K i_{sD}, i_{sQe} = \sum i_{sQ} = K i_{sQ}. \quad (13)$$

This article has been accepted for publication in a future issue of this journal, but has not been fully edited. Content may change prior to final publication. Citation information: DOI 10.1109/TSG.2019.2907600, IEEE Transactions on Smart Grid

As the stator voltage keeps unchanged, the stator and rotor flux of the equivalent IM are obtained as:

$$\psi_{rDe}=\psi_{rD},\psi_{rQe}=\psi_{rQ},\psi_{sDe}=\psi_{sD},\psi_{sQe}=\psi_{sQ}. \quad (14)$$

According to the second condition, the load torque and rotor angular velocity are:

$$\omega_{re}=\omega_r,T_{Le}=\sum T_L=KT_L. \quad (15)$$

From the third condition, the electrical parameters of the equivalent IM should meet the relationship below:

$$T_{se}=T_s=L_s/R_s,T_{re}=T_r=L_r/R_r. \quad (16)$$

Substituting (13-16) into the flux and voltage equations (7-11), the parameters of the equivalent motor load rated at P_{IM}=KP_nW can be described by an IM load factor K:

$$L_{me}=L_m/K,L_{se}=L_s/K,R_{se}=R_s/K,L_{re}=L_r/K,\\ R_{re}=R_r/K,J_e=KJ,T_{Le}=KT_L \quad (17)$$

Therefore, based on a typical motor load rated at P_nW, the parameters of the equivalent motor load rated at P_{IM}=KP_nW can be described by (17). Thus, the continuous increment of IM load is described by increasing load coefficient *K*.

C. Model of ZIP Load

ZIP loads are often used in static analyses and are packaged in many commercial software tools (such as PSCAD and Matlab/SimPowerSystems.). The load consumption of ZIP load can be represented by the polynomials as:

$$P_{ZIP}=P_0(a_1\frac{U_b^2}{U_0^2}+a_2\frac{U_b}{U_0}+a_3),Q_{ZIP}=Q_0(b_1\frac{U_b^2}{U_0^2}+b_2\frac{U_b}{U_0}+b_3), \quad (18)$$

where P_0 and Q_0 are the nominal active-power and reactive-power, respectively under the nominal voltage U_0. a_1 and b_1, a_2 and b_2, and a_3 and b_3 are the percentages of the constant-impedance load, constant-current load, and constant-power load, respectively, and U_b denotes the magnitude of bus voltage.

Instead of active and reactive power flows, the line currents are used as the signal flows in the network of microgrid model for describing the line dynamics. Thus, the equation (18) cannot be integrated in MG model directly. Therefore, the parallel combination of conductance G_{ZIP} and susceptance B_{ZIP} are used to present ZIP load model depicted in Fig. 3. The G_{ZIP} and B_{ZIP} can be described as:

$$G_{ZIP}=P_0(\frac{a_1}{U_0^2}+\frac{a_2}{U_0U_b}+\frac{a_3}{U_b^2}),B_{ZIP}=-Q_0(\frac{b_1}{U_0^2}+\frac{b_2}{U_0U_b}+\frac{b_3}{U_b^2}). \quad (19)$$

From (18), the values of G_{ZIP} and B_{ZIP} depend on the magnitude of bus voltage U_b. The state equations of the ZIP load current can be written on the common reference frame as:

$$\tau\dot{i}_{Pd}=G_{ZIP}u_{bd}-i_{Pd},\tau\dot{i}_{Pq}=G_{ZIP}u_{bq}-i_{Pq}. \quad (20)$$

The state equations of the load current of B_{ZIP} can be presented on the common reference frame as:

$$\tau\dot{i}_{Qd}=-B_{ZIP}u_{bq}-i_{Qd},\tau\dot{i}_{Qq}=B_{ZIP}u_{bd}-i_{Qq}. \quad (21)$$

where τ is defined as the time constant of ZIP load.

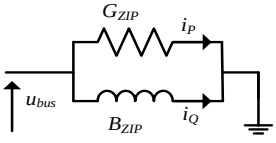

Fig. 3. Equivalent circuit of a ZIP load.

D. Model of Microgrid System

To extract all the dynamics in the proposed system, the dynamics of the connecting line between the bus *i* and bus *j* can be described as:

$$\dot{i}_{lineD}=(u_{biD}-u_{bjD}-R_{line}i_{lineD}+\omega_{com}L_{line}i_{lQ})/L_{line} \quad (22)$$

$$\dot{i}_{lineQ}=(u_{biQ}-u_{bjQ}-R_{line}i_{lineQ}-\omega_{com}L_{line}i_{lineD})/L_{line} \quad (23)$$

To define the bus voltage well, a small virtual capacitor C_{vir} is added between the bus and ground. The voltage of bus *i* can be written as:

$$\dot{u}_{bDi}=(\sum i_{oD}-\sum i_{loadD}+\sum i_{lineD}+\omega_{com}C_{vir}u_{bQi})/C_{vir} \quad (24)$$

$$\dot{u}_{bQi}=(\sum i_{oQ}-\sum i_{loadQ}+\sum i_{lineQ}-\omega_{com}C_{vir}u_{bDi})/C_{vir} \quad (25)$$

The dynamic model of MG is organized as differential-algebraic equations. The islanded MG with *m* DGs, *n* lines, *k* IM loads, *l* ZIP loads, and *i* buses has $13m + 2n + 5k + 4l + 2i$-1 state variables to describe its dynamics.

III. Parameter Stability-Region Analysis Based on Bifurcation Theory

A. System Description

In this section, the numerical bifurcation method is applied to analyze the parameter stability region of a microgrid system. The microgrid system is as shown in Fig. 4, which consists of two droop-controlled DGs, a dynamic IM load, and a static ZIP load. DGs and loads are connected through a tie-line with inductance L_{line} and resistance R_{line}.

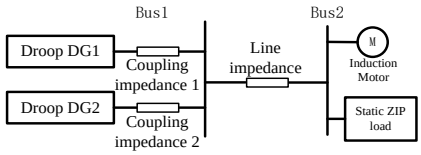

Fig. 4. The microgrid with 2 DGs.

In this MG, the parameters of the two droop-controlled DGs are given in Table I, and the load parameters under the rated operation condition are given in Table II. The inductance and resistance of connection lines are 0.26mH/km and 0.164Ω/km respectively. The length of connection line L_{line}=0.5 km.

TABLE I. Droop-Controlled DG Parameters

Parameter	Value	Parameter	Value
P_{n1}, P_{n2}	40 kW, 20 kW	L_{f1}, L_{f2}	1.2 mH, 1.2 mH
U_{n1}, U_{n2}	330 V, 330 V	R_{f1}, R_{f2}	0.1 Ω, 0.1 Ω
m_{p1}, m_{p2}	0.75e^{-4}rad/W, 1.5e^{-4} rad/W	C_{f1}, C_{f2}	0.55 mF, 0.45 mF
m_{q1}, m_{q2}	5e^{-4}V/Var, 7e^{-4}V/Var	L_{q1}, L_{q2}	0.6 mH, 0.4 mH
ω_c	31.4 rads/s	R_{q1}, R_{q2}	0.3 Ω, 0.2 Ω
K_{vp1}, K_{vp2}	1.2, 1	K_{cp1}, K_{cp2}	4, 3.2
K_{vi1}, K_{vi2}	380, 275	K_{ci1}, K_{ci2}	550, 480

TABLE II. Load Parameters

ZIP load parameter	Value	IM load parameter (22.5kW)	Value
b_1, b_2, b_3	0.2,0.3,0.5	L_m	0.043927 mH
c_1, c_2, c_3	0.2.0.3.0.5	L_r, R_r	0.0449 mH, 0.228 Ω
P_0	10kW	L_s, R_s	0.0449 mH, 0.087 Ω
Q_0	5kVar	J	1.662 kgm^2
U_0	311V	T_0, T_1, T_2	65, 0.5, 0

Bifurcation analysis is a powerful tool to analyze the parameter stability of nonlinear system. The occurrence of local

This article has been accepted for publication in a future issue of this journal, but has not been fully edited. Content may change prior to final publication. Citation information: DOI 10.1109/TSG.2019.2907600, IEEE Transactions on Smart Grid

bifurcation leads the nonlinear system to become unstable. In general, bifurcations are caused by continuous variations of one or more parameters. Using the bifurcation analysis package software MATONT [28], the bifurcation boundaries and solution manifolds of different parameters are plotted. For electrical power system, Hopf bifurcation (HB) and saddle-node bifurcation (SNB) are the major local stability boundaries [18-19]. When SNB occurs, a real eigenvalue is located on the imaginary axis. If the parameters continue to change, the stable equilibrium disappears and the system collapses. When HB occurs, a pair of complex conjugate eigenvalues are on the imaginary axis. After that, the limit circle will emerge, and then the system becomes oscillatory.

B. Case1: Bifurcation Analysis on m_p-m_q Plane

The power controller of droop-controlled DG dominates the dynamic behavior of the microgrid. The scheduling of the power droop gains determines the power regulation of microgrids. In this part, the parameters of power controllers including active power gain m_p and reactive power gain m_q, are selected to do bifurcation analysis. The influences of cut-off frequency, coupling inductor, and load on the stability region of microgrid are investigated. The starting point of the bifurcation analyses is the equilibrium of MG with the parameters in Table I and Table II. To ensure the power sharing of the two DGs, the ratio between the active power gains of two DGs is maintained at 1:2, and the ratio between the reactive power gains is maintained at 5:7.

Fig. 5 plots the bifurcation diagram of m_p and m_q, where the red curves denote the HB boundaries of test system, respectively. Two HB boundaries bound the parameter stability region on m_p-m_q plane. The proposed MG tends to lose its stability with the increase of m_p or m_q. The Lyapunov coefficients on the two HB curves are smaller than 0. Thus, increasing m_p or m_q will lead to the subcritical HB1 and HB2, respectively. Besides, increasing reactive-power droop gain m_q extends the upper limit value of active power gains m_p. While m_p has little effect on the upper limit of m_q and raise the lower limit of m_q. The feasible region of m_q narrows when m_p increases. Thus, when a large m_p is designed to improve transient response, a large m_q should be selected to make sure the stability of MG.

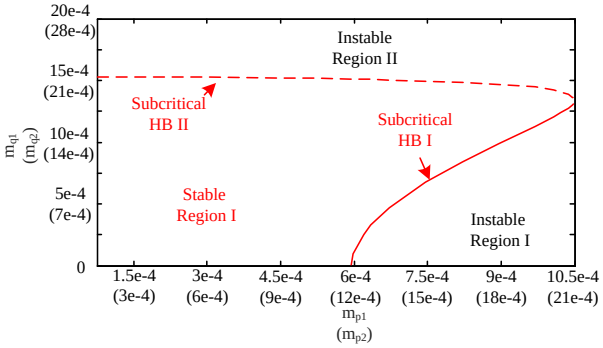

Fig. 5. The parameter stability region on m_p-m_q plane.

In [21], the stable region of MG with resistance load is plotted on m_p-m_q using the small-signal analysis. The unstable phenomena are also founded in this test MG model, which are identified as HB phenomena. The phase plane of active power P_1 and reactive power Q_1 before and after subcritical HB1 are plotted in Fig. 6. The red curve denotes the trajectory of operation point before the subcritical HB1 when m_{p1} = 4.5e^{-4}, m_{q1} = 5e^{-4} (m_{p2} = 9e^{-4}, m_{q2} = 7e^{-4}). The blue curve denotes the trajectory after the subcritical HB when m_{p1} = 7.5e^{-4}, m_{q1} = 5e^{-4} (m_{p2} =15e^{-4}, m_{q2} =7e^{-4}). The subcritical HB1 gives rise to an unstable limit circle around the stable equilibrium. As illustrated, the trajectory after the HB diverges from the start point, and the system becomes oscillatory.

Then, the impacts of the cut-off frequency ω_c on the stability region of m_p-m_q plane are studied. The cut-off frequency of two DGs are both changed. It can be seen from Fig. 7, decreasing the inverter cut-off frequency ω_c broadens the stability region. Besides, the extension part of the stability region is the area with a larger reactive power gain m_q. The extended range of the active power droop gain is only valid when the reactive droop gain increases correspondingly.

Fig. 8 plots the stability region on m_p-m_q plane when different coupling inductors are selected. As presented in Fig 8, the increase of coupling inductance tends to increase the overall stability region on m_p-m_q plane, especially in terms of active power gain. That means a weaker coupling between inverters will improve the system stability. It can be noticed that not only a greater inductor but also a substantial virtual impedance can be utilized to broaden the parameter stability region.

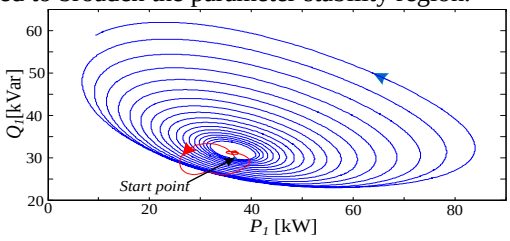

Fig. 6. Phase plane of the microgrid before and after subcritical Hopf bifurcation. Red curve: stable operation; Blue curve: subcritical Hopf bifurcation.

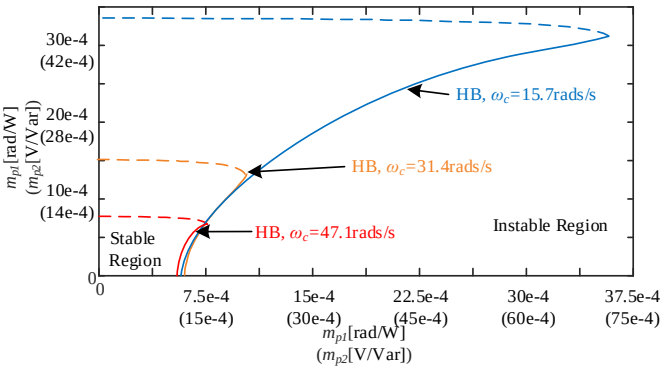

Fig. 7. Hopf bifurcation boundaries for MG with different cut-off frequency.

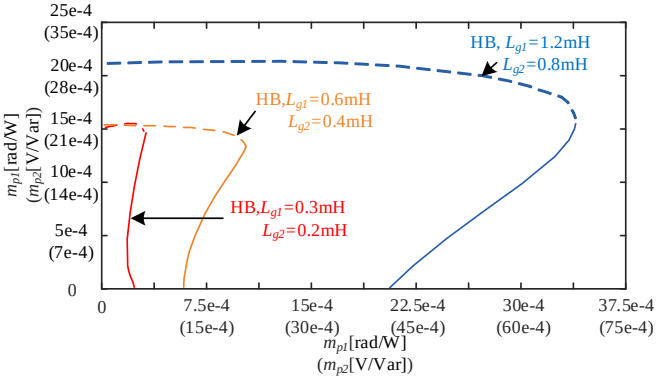

Fig. 8. Hopf bifurcation boundaries for MG with different coupling inductance.

This article has been accepted for publication in a future issue of this journal, but has not been fully edited. Content may change prior to final publication. Citation information: DOI 10.1109/TSG.2019.2907600, IEEE Transactions on Smart Grid

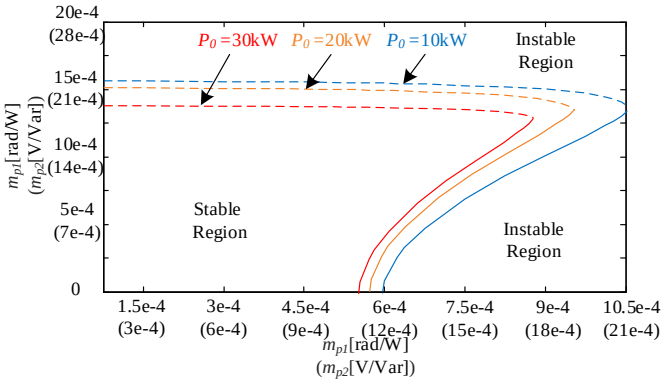

Fig. 9. Hopf bifurcation boundaries for MG with different ZIP load.

Fig. 9 plots the parameter stability region on m_p-m_q plane when the active power of ZIP load increases from 10kW to 30kW. The stable region of MG shrinks with the increase of ZIP load. The increasing active power load has minor effect on m_q but narrows the stability region of m_p.

C. Case 2: Bifurcation Analysis on P-V plane

For the MG in islanded mode, the power assumption of a local load can only be provided by the inverter-based DGs. Power unbalance is the major physical mechanism of instability, the maximum power supply of MG should be calculated to make sure its stability. In this part, the bifurcation analyses are performed on P-V plane. The influences of connection line, virtual inductance, reactive power controller on the parameter stability region are investigated.

As presented previously that the parameter stability region on m_p-m_q plane is highly related to the coupling inductor of inverters. Thus, a large inductor is recommended for improving the stability of microgrid with parallel inverters. However, the installation of bulk inductor is costly. Thus, virtual impedance control has been proposed in the literatures [29] for stability improvement, harmonic mitigation and also for fault ride through. In general, the voltage droop from the virtual inductor that reacts to output current is added on the voltage reference. The modified voltage references can be presented by

$$\begin{aligned} u_{odi}^{ref} &= U_n - m_{qi}Q_i + \omega_0 L_{vi} i_{oqi} - R_{vi} i_{odi} \\ u_{oqi}^{ref} &= -\omega_0 L_{vi} i_{odi} - R_{vi} i_{oqi} \end{aligned} \tag{26}$$

This section discusses the parameter stability region of MG when virtual inductor control is implemented. The physical coupling impedance of inverter 1 and 2 are designed as 0.3+j0.24πΩ and 0.2+j0.16πΩ, respectively. The virtual inductor of inverters L_{vir} is initially set to 4mH.

Fig. 10 plots the equilibrium solution manifold for different types of load on the active-power versus bus voltages (P-V) plane. The nominal reactive-power Q_0 is set to zero. The constant-impedance load, constant-current load, and constant-power load are obtained by setting percentages of ZIP load as a_1, b_1 = 100%; a_2, b_2 = 100%, and a_3, b_3 = 100%, respectively. It can be seen from Fig. 10 that the voltage at bus 2 decreases when the load increases. Then, an SNB point is found in the equilibrium solution manifold of the constant-power load when P_0 = 58.17 kW. An SNB point can also be found in the curve for IM load when the IM load P_{IM} = 42.54 kW. The PCC voltage decreases sharply when the load close to the SNB boundary and their bifurcation point of PCC voltage are around 200V, which indicates the voltage instability phenomenon. The stable equilibrium will disappear after the SNB, and the nonlinear system loses its stability when the SNB occurs. For the bifurcation curves of constant-impedance and constant-current loads, the bifurcation phenomena do not exist. Therefore, in a ZIP load model, the constant-power component has a significant effect on the stability of MG. In addition, the stability margin of IM load is smaller than that of ZIP load.

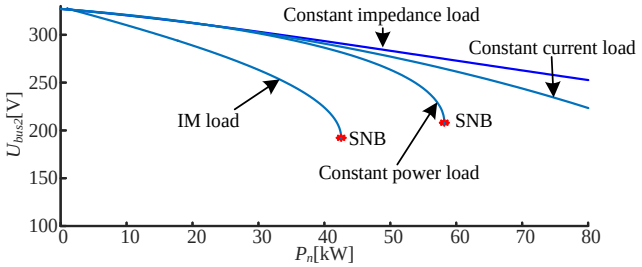

Fig. 10. Equilibrium solution manifold on the P_0-U_{bus2} plane for load increasing. SNB is saddle-node bifurcation detected in the curve of IM load and constant-power load.

Fig. 11 presents the influence of the connection line with fixed X/R ratio. The increasing the length of connection line tends to shrink the stability region. Besides, the parameter stability region of IM loads is smaller than that of constant power load. As shown in Fig. 12, the increase of virtual coupling inductor moves the SNB boundary to a lower level. Thus, the application of virtual inductance control tends to broaden the parameter stability region on m_p-m_q plane, but shrinks the stability region on P-V plane. That means, both SNB and Hopf boundaries should be considered for virtual inductance design to keep the safe operation of the microgrid.

Since, the power assumption is related to the voltage regulation. The influence of reactive-power droop control on the SNB is investigated. The Fig. 13 plots stability region of m_q when virtual inductor is added. In this case, the SNB occurs before the HB for a relatively large load consumption. Moreover, the m_q limit decrease sharply with load increase. A small value of reactive power gain should be designed for improving the stability when system under heavy load condition. For the m_q design, there is a trade-off between the accurate reactive-power sharing and maximum power transmission. Fig. 14 plots the SNB when nominal voltage change. It can be seen that decreasing nominal voltage shrink the stable range of load assumption. Since, the nominal voltage may be scheduled on secondary control level, its stable range should be fully evaluated.

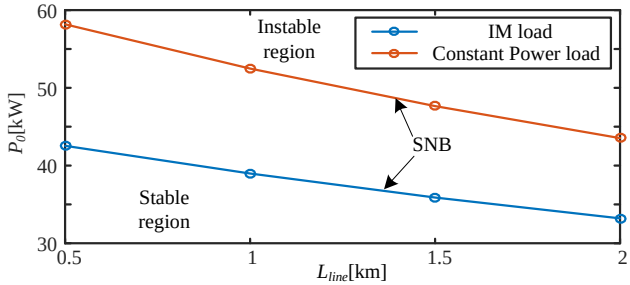

Fig. 11. SNB boundaries for MG with different lengths of connection line.

This article has been accepted for publication in a future issue of this journal, but has not been fully edited. Content may change prior to final publication. Citation information: DOI 10.1109/TSG.2019.2907600, IEEE Transactions on Smart Grid

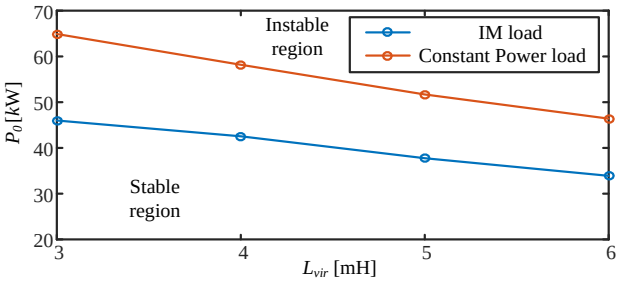

Fig. 12. SNB boundaries for MG when different virtual inductances are selected.

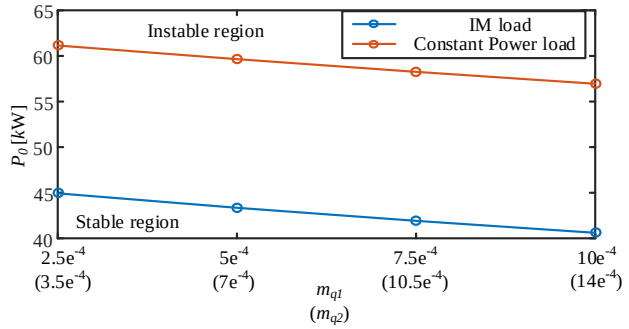

Fig. 13. SNB boundaries of P_0 for MG when different reactive-power droop gain m_q are selected.

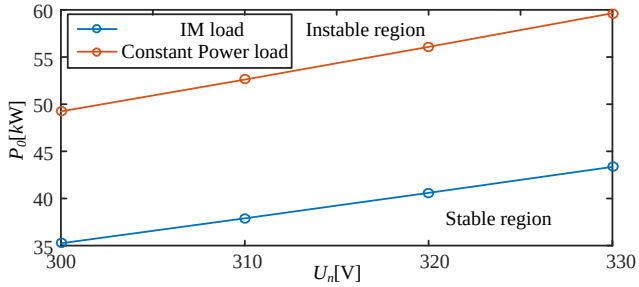

Fig. 14. SNB boundaries of P_0 for MG when different nominal voltage of droop controller U_n are selected.

From the bifurcation analysis above, several conclusions are obtained as follows:

1) For the MG with ZIP loads and induction motor loads, increasing the active power gain m_p or reactive power gain m_q leads to the subcritical HB phenomena. MG becomes oscillating after the subcritical HB whose boundaries constitute the parameter stability region on the m_p-m_q plane. Decreasing the value of cut-off frequency ω_c or increasing the value of coupling inductance broadens the parameter stability region on m_p-m_q plane. The connected loads have minor effect on the HB boundaries.

2) The increase of an IM load or constant power component of a ZIP load results in the SNB phenomena. The bus voltages of the microgrid collapse after the SNBs. SNB boundaries constitute the parameter stability region for load increasing. Decreasing the value of reactive power gain m_q or impedance of connection line will broaden the stability region of loads. Increasing the value of nominal voltage U_n or virtual inductance shrink the stability region of load.

IV. Reduced Order Model for the Bifurcation Analysis

In section III, the parameter stability region analysis of the proposed microgrid is carried out using the full-order model, which is complex and brings huge computation burdens for plotting the bifurcation boundaries. For a microgrid in operation, the plotted stability region can be used to predict the stability margin according to its current state, which is useful for the on-line scheduling of control parameters. Thus, reducing the computation time is the key to make sure the timely response of DG. In this section, reduced-order models of the MG are developed to improve the computation efficiency for bifurcation analysis.

The singular perturbation method can reduce the order of dynamic model by eliminating the dynamics from part of state variables. As bifurcation phenomenon is activated by changing a specific parameter, in this section, the reduced models are developed to analyze the stability region in terms of control parameters and loads. The reduced model for a bifurcation phenomenon preserves the state variables that are highly related to this bifurcation.

The procedure of the model order reduction is as shown in Fig. 15. The MG can be divided into several subsystems whose dynamic behavior are described by a set of state variables. The state variables from the bus voltage are not included due to their negligible influence on the system dynamics. Table III presents the classified subsystem and their corresponding state variables. The subsystems are classified into fast and slow subsystems according to the participation analysis results. The dynamics from the slow subsystem will be preserved in the final reduced model.

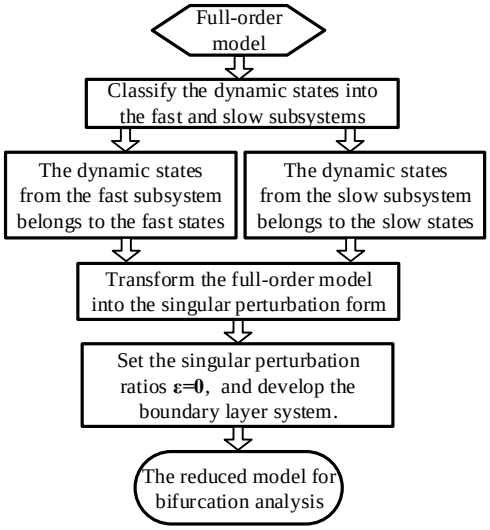

Fig. 15. The procedure of model order reduction.

The major participants of dominant modes are preserved in all reduced models to define the equilibrium of the MG model. HB as a dynamic bifurcation can be detected when a pair of eigenvalues pass through the imaginary axis. Therefore, the state variables related to these eigenvalues need to be preserved in the reduced model for HB calculation. Participation analysis is applied to identify the state variables associated with bifurcation phenomenon. The participation factor is a measure of the relative participation of the kth state variable in the ith mode, and vice versa. The participation factor of the ith mode and jth state is given by:

$$p_{ij} = \frac{\left|u_{ij}^{T}\right|\left|v_{ij}\right|}{\sum_{k=1}^{N}\left|u_{kj}^{T}\right|\left|v_{jk}\right|} \tag{27}$$

where u_{ij} and v_{ij} denotes the left eigenvectors and right eigenvectors, respectively. The participation of a subsystem on the mode i is defined by summing up all participation factors of

This article has been accepted for publication in a future issue of this journal, but has not been fully edited. Content may change prior to final publication. Citation information: DOI 10.1109/TSG.2019.2907600, IEEE Transactions on Smart Grid

dynamic states describing this subsystem, which can be written as:

$$p_{i,set\_k} = \sum_{i,\, j \in set\_k} p_{ij} \tag{28}$$

where the subscript *set_k* denotes the subsystem described by the state variables in *set_k*.

The effects of the subsystem on the dominant eigenvalues are presented in Table IV. It can be observed that the major participants of dominant eigenvalues are the dynamics from the power controllers and IM loads. The boundary of HB1 shown in Fig. 5 is dominated by a pair of eigenvalues $\lambda_{2\text{-}3}$. In addition to the dynamics from power controllers, the network dynamic has considerable effect on $\lambda_{2\text{-}3}$. The boundary of HB2 is dominated by the pair of eigenvalues $\lambda_{7\text{-}8}$. The dynamics from the inner controller loop, network and power controller have considerable effect on $\lambda_{7\text{-}8}$. The reduced models for predicting different bifurcation boundaries are organized in Table V. Because the slow states in the two DGs are the same, these states will not be presented in twice.

TABLE III. DYNAMICS OF MG

Subsystem of MG	Dynamics states sets
Power Controller of DGs	θ_2 , P, Q
Inner control loop of DGs	φ_d, φ_q, u_{od}, u_{oq}, γ_d, γ_q, i_{ld}, i_{lq}
Network dynamics	i_{od}, i_{oq}, i_{lined}, i_{linq}
IM load	Ψ_{rD}, Ψ_{rQ}, ω, i_{sd},i_{sq}
ZIP load	i_{pd},i_{pq},i_{qd},i_{qq}

TABLE IV. PARTICIPATION ANALYSIS RESULT

Index	Eigenvalues	Participant dynamics (participation factor)
λ_1	-9.8	Rotor side dynamics of IM (0.93)
$\lambda_{2\text{-}3}$	-11.9 ± j53.2 (HB1)	Power controller (0.86), Network dynamics (0.11)
λ_4	-29.8	Power controller (0.92)
λ_5	-37.3	Power controller (0.85), Rotor side dynamics of IM (0.13)
λ_6	-42.3 ± j50.1	Rotor side dynamics of IM (0.83)
$\lambda_{7\text{-}8}$	-56.1 ± j253. 1(HB2)	Inner Control Loop (0.45), Network Dynamics (0.44), Power controller (0.1)

TABLE V. REDUCED MODEL FOR BIFURCATION ANALYSIS

Bifurcation boundaries	Dynamics preserved in the reduced model	Slow states in the reduced model	Order of the reduced model
SNB with increasing load	Power controller, IM load	θ_2 , P, Q, Ψ_{rD}, Ψ_{rQ}, ω, i_{sd}, i_{sq}, u_{bD}, u_{bQ}	14
HB1 with increasing m_p	Power controller, IM load Line dynamics	θ_2 , P, Q, Ψ_{rD}, Ψ_{rQ}, ω, i_{sd}, i_{sq} i_{od}, i_{oq}, i_{lined}, i_{linq}, u_{bD}, u_{bQ}	20
HB2 with increasing m_q	Power controller, IM load, Line dynamics, Inner control loop	θ_2 , P, Q, Ψ_{rD}, Ψ_{rQ}, ω, i_{sd},i_{sq} i_{od}, i_{oq}, i_{lined}, i_{linq}, u_{od}, u_{oq}, i_{ld}, i_{lq}, φ_d, φ_q, γ_d, γ_q, u_{bD}, u_{bQ}	36

Then, the dynamic model of the MG can be rewritten in a singular perturbation form as:

$$\dot{\boldsymbol{x}} = \boldsymbol{f}(\boldsymbol{x},\boldsymbol{z},t,\varepsilon) \tag{29}$$

$$\varepsilon\dot{\boldsymbol{z}} = \boldsymbol{g}(\boldsymbol{x},\boldsymbol{z},t,\varepsilon) \tag{30}$$

where $\varepsilon = \mathrm{diag}\{\varepsilon_1, \varepsilon_2, \ldots, \varepsilon_m\}$ denotes a diagonal matrix whose elements are the ratios of physical parameters that reflect the "true smallness" [23]. Subsequently, the state equations of the fast state variables (30) are transformed into the boundary layer system by setting ε to be 0, and the quasi-steady-state solution of fast states are presented by x as:

$$z = h(x, t) \tag{31}$$

Finally, the reduced dynamic model can be obtained by substituting (31) into (29) as:

$$\dot{\boldsymbol{x}} = \boldsymbol{f}(\boldsymbol{x},\boldsymbol{h}(\boldsymbol{x},t),t,0) \tag{32}$$

Thus, the slow dynamics of the original system are preserved in (32), and the original fast states can be described by the algebraic equation (31). The boundary layer system for the SNB is presented in the Appendix.

The bifurcation analysis is performed to compare the calculation times of the reduced-order models with those of the full-order model. The start point is the equilibrium of the MG with the parameters in Table I and Table II. The reduced model for SNB is used to predict the SNB point with load increasing as shown in Fig. 10. The calculation times of bifurcation boundary based on the reduced models are much smaller than those based on the full-order models.

TABLE VI. COMPARISON OF TIME FOR BIFURCATION ANALYSIS

Case	Calculation time for the proposed reduced model	Calculation time for the full-order model
SNB (Increase of IM loads)	14.6s	37.8s
SNB (Increase of constant power loads)	17.5s	55.4s
HB1 (Increase of active power gain m_p)	2.2s	13.3s

To validate the accuracy of the reduced model, the calculation error of the proposed model is compared with that of the reduced models in [21] and [23], as presented in Table VII. The error of the reduced model is measured as:

$$\boldsymbol{error} = \left| \frac{\lambda_{re} - \lambda_{full}}{\lambda_{full}} \right| \times 100\% \tag{33}$$

where λ_{full} and λ_{re} denotes the bifurcation parameter of full-order model and reduced model at the bifurcation point, respectively. In [21, 23], the general reduced model for different cases is designed. In [21], the dynamics from the power controller and connection line are preserved in the reduced model. [23] preserves the dynamics from the power controller and inner control loop. The proposed models are more accurate than the general reduced model which indicates that for a specific bifurcation phenomenon, the corresponding reduced model should be designed for an accurate result.

TABLE VII. COMPARISON OF ERRORS FOR BIFURCATION ANALYSIS

Case	Proposed Models	Reduced model in [21]	Reduced model in [23]
SNB (Increase of ZIP loads)	0	0	0
HB1 (Increase of active power gain m_p)	9.6%	9.6%	17.1%
HB2 (Increase of active power gain m_q)	2.3%	29.8%	12.1%

V. VERIFICATION

A. Simulation Results

In this section, the bifurcation phenomena and the parameter stability region analysis are validated using the switching testbed of the proposed MG built in the MATLAB/SymPowerSystem environment. The parameters

This article has been accepted for publication in a future issue of this journal, but has not been fully edited. Content may change prior to final publication. Citation information: DOI 10.1109/TSG.2019.2907600, IEEE Transactions on Smart Grid

from Tables I and II are used. To validate the parameter stability region composed of HB boundaries, the simulation results when active power gains m_{p1} and m_{p2} switch from m_{p1} = 1.5e^{-4} and m_{p2} = 3e^{-4} to m_{p1} = 7.5e^{-4} and m_{p2} = 15e^{-4} coordinately at 3 s are shown in Fig. 16. The waveform starts to oscillate at 3 s, after which the magnitude of the oscillation gradually become larger. This kind of nonlinear phenomenon belongs to the subcritical HB, and coincides with the analysis in Section III.

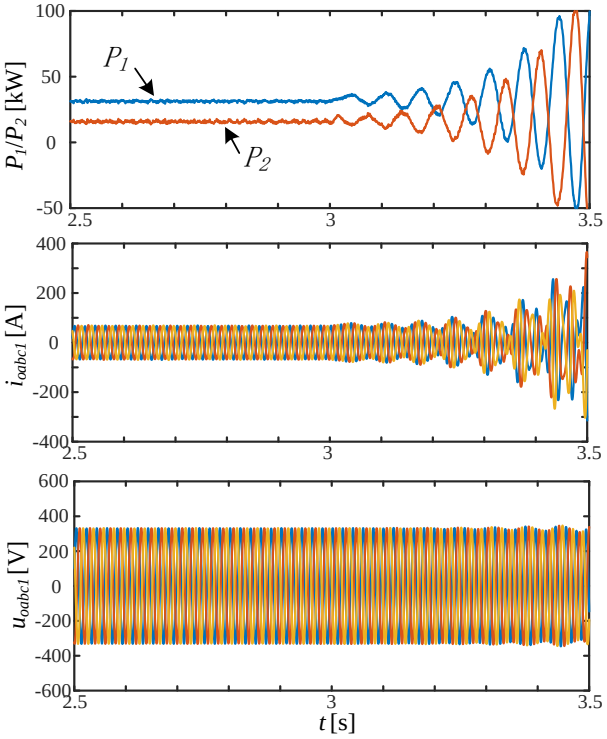

Fig. 16. Simulation results of DG1 when the active gains are switched from m_{p1} = 1.5e^{-4} and m_{p2} = 3e^{-4} to m_{p1} = 7.5e^{-4} and m_{p2} = 15e^{-4} at 3 s

The parameter stability region of the ZIP load shown in Fig. 10 is validated by the simulation results, as shown in Fig. 17. The active power in the ZIP load continuously increases by connecting the input reference value port of the load module in MATLAB/SymPowerSystem to a ramp signal source. When the ZIP load is composed of a 100% constant-power load component, the voltage decreases and collapses at 3.2 s. Fig. 19 shows the voltage at bus 2 with a 37.5-kW IM load in large time scale. The parameters of this IM load are designed according to Table II. At 2 s, a 15-kW IM load with an IM load factor K = 15/22.5 is connected to bus 2. The bus voltage decreases continuously after the step change of IM load, and the angular velocity will eventually decrease to 0 rads/s.

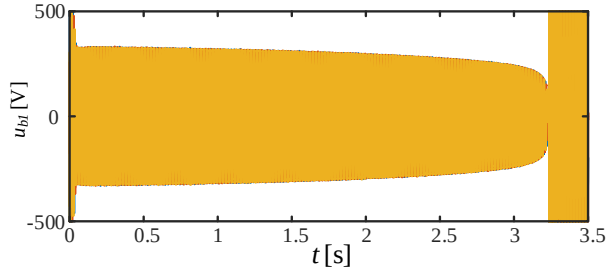

Fig. 17. The phase voltage at bus 2 with the increase of the rated active power at a ZIP load that consists of 100% constant active power load. The SNB appears and then system collapses.

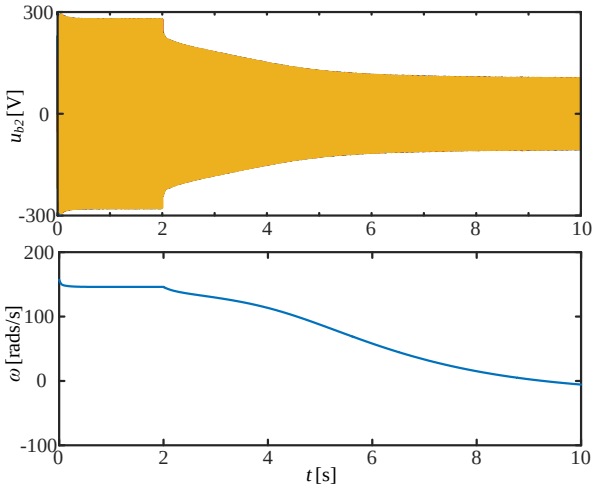

Fig. 18. The phase voltage at bus 2 with the increase of the IM load. The system collapses and SNB appears after the connection of the 15 kW IM load.

Fig. 19 is plotted to validate the influence of virtual inductance control and droop control on the SNB boundaries. The constant power load with 50kW nominal active power is connected to bus 2. In Fig. 19(a) the virtual inductance is switched from 4mH to 6mH at 2s, the voltage collapse after 2s. In Fig. 19(b), the nominal voltage in power controller is switched from 330V to 300V at 2s, the bus voltage continuously decrease, and eventually collapse after 3.3s.

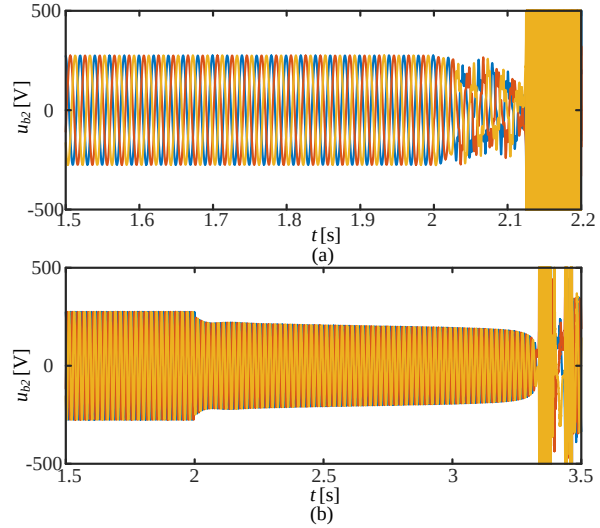

Fig. 19. The phase voltage at bus 2 with 50kW ZIP load. (a) The virtual inductance of is switched from 4mH to 6mH at 2s. (b) The nominal voltage of droop controller is switched from 330V to 300V at 2s.

B. Experimental Results

The hardware in-the-loop (HIL) method is proposed for the experiment verification in this section. All the electrical components including power electronic inverters, network, ZIP load and IM load are simulated at real time in RT-LAB [30]. The two droop-controlled inverters are controlled via two real DSP controllers, respectively. The parameters of droop controllers and electrical circuit are the same as shown in Table I and Table II.

Fig. 20 shows the waveforms of the DG1 after the subcritical HB. The active power gains of two DG m_{p1} and m_{p2} are switched from m_{p1} = 1.5e^{-4}, m_{p2} = 3e^{-4} to m_{p1} = 7.5e^{-4}, m_{p2} = 15e^{-4} coordinately. Since the output ranges of the analog out ports are

This article has been accepted for publication in a future issue of this journal, but has not been fully edited. Content may change prior to final publication. Citation information: DOI 10.1109/TSG.2019.2907600, IEEE Transactions on Smart Grid

limited, the maximum permissible magnitude of output current signals is 100 A. The output voltages and currents of the DGs fluctuate after the subcritical bifurcation, which coincides with the bifurcation analysis and the simulation results.

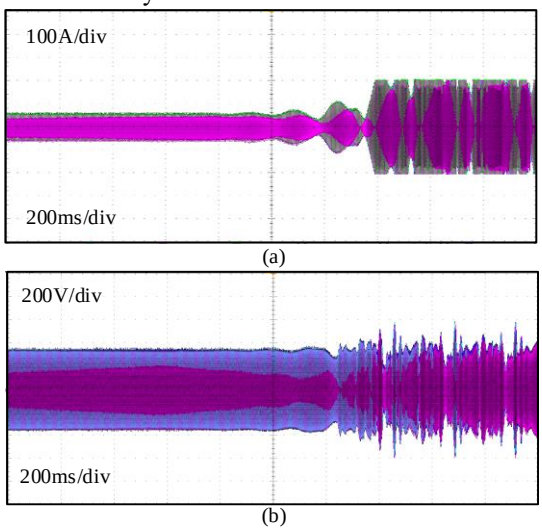

Fig. 20. Experiment results of the subcritical HB. (a) Output currents. (b). Output voltages.

Fig. 21 shows the experiment result of the SNB as load increases. The voltage of Bus 2 decreases with the continuous increment of the constant power load, and eventually, the voltage collapses. This result is in accordance with the simulated result given in Fig. 18 and Fig. 19. The SNB phenomenon caused by the increment of the IM load is verified. A 37.5 kW IM load is connected to the Bus 2 at first. Then, a 15 kW IM load is integrated. The voltage of Bus 2 droops irreversibly, which coincides with the simulation result as shown in Fig. 19.

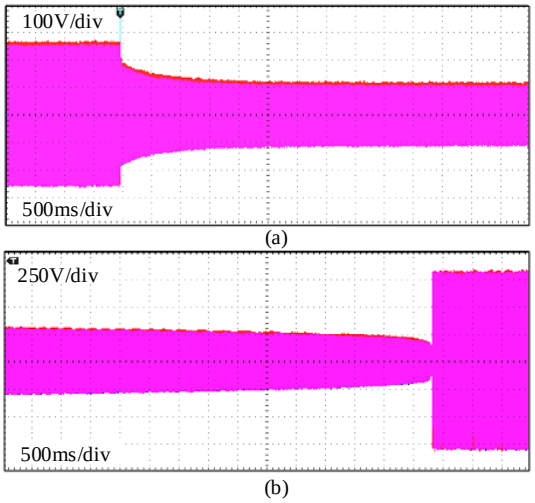

Fig. 21. Experiment results of the SNBs. (a) The IM load steps from 37.5 kW to 52.5kW. (b) Constant active-power load increases.

VI. Conclusion

This paper studies the modeling and parameter stability region analysis of a droop-controlled MG with dynamic IM load and static ZIP load. Reduced-order models for parameter stability region analysis are presented based on the singular perturbation method. Several conclusions are obtained.

1) The equivalent model of ZIP load and IM load are developed to combine a complete model of MG, which can describe the load increasing for bifurcation analyses.

2) The SNB and HB boundaries constitute the parameter stability region of MG with ZIP and IM load. The HB of power droop gain are related to dynamics from the power controller and network of DGs. The SNB of load are related to the coupling inductance, connection line and voltage control.

3) The reduced-order models for numerical bifurcation analysis predicts the bifurcation phenomena with low computation burden. The dynamics of power controllers and IM loads have major influence on the SNB with load increasing and should be preserved in the reduced model for predicting SNB. The reduced model for predicting the HB with the change of active-power droop gain should preserve the dynamics of power controllers, IM loads and network dynamics. The reduced model for predicting the HB with the change of reactive-power droop gain can only eliminate the dynamics of ZIP loads.

Appendix

The boundary layer system of the reduced model is presented in this section. According to the description on section IV, the differential equations of fast states are degraded to the algebraic equations. The algebraic part of the reduced model for predicting the SNB that eliminates most dynamics of subsystems is presented in detail. After classifying the dynamic states into the slow-state vector x and fast-state vector z, the state equations of inner control loop, line dynamics and ZIP load are normalized as the singular perturbation form zoo as:{ $\frac{1}{K_{vi}}\varphi_d$, $\frac{1}{K_{vi}}\varphi_q$, $C_f u_{odi}$, $C_f u_{oqi}$, $\frac{1}{K_{ci}}\gamma_d$, $\frac{1}{K_{ci}}\gamma_q$, $\frac{L_f}{R_f}i_{ldi}$, $\frac{L_f}{R_f}i_{lqi}$, τi_{GD} , τi_{GQ} , τi_{BD} , τi_{BQ} , $\frac{L_g}{R_g}i_{od}$, $\frac{L_g}{R_g}i_{oq}$, $\frac{L_{line}}{R_{line}}i_{lined}$, $\frac{L_{line}}{R_{line}}i_{lineq}$ }. By setting ε = 0, the dynamic equations of the fast states degenerate into the boundary layer system. Then, Gaussian elimination is applied to obtain the quasi-steady-state solution of fast states.

The inner control loop can be presented in algebraic form as:

$$u_{od} = \mathrm{U}_n - n_q Q,\ u_{oq} = 0\,, \tag{A1}$$

$$i_{ld} = i_{od}\,, i_{lq} = i_{oq} + \omega C_f(\mathrm{U}_n - n_q Q)\,. \tag{A2}$$

The output current can be written in algebraic form by

$$i_{oD} = \frac{R_g(u_{oD} - u_{bD}) + \omega_{com} L_g(u_{oQ} - u_{bQ})}{R_g^2 + \omega_{com}^2 L_g^2}, \tag{A3}$$

$$i_{oQ} = \frac{R_g(u_{oQ} - u_{bQ}) - \omega_{com} L_g(u_{oD} - u_{bD})}{R_g^2 + \omega_{com}^2 L_g^2}. \tag{A4}$$

The line current between bus1 and bus2 can be written as:

$$i_{lineD} = \frac{R_{line}(u_{b1D} - u_{b2D}) + \omega_{com} L_{line}(u_{b1Q} - u_{b2Q})}{R_{line}^2 + \omega_{com}^2 L_{line}^2}, \tag{A5}$$

$$i_{lineQ} = \frac{R_{line}(u_{b1Q} - u_{b2Q}) - \omega_{com} L_{line}(u_{b1D} - u_{b2D})}{R_{line}^2 + \omega_{com}^2 L_{line}^2}. \quad \text{(A6)}$$

The ZIP load is presented in algebraic form as:

$$i_{PD} = G_{ZIP} u_{bD}, \quad i_{PQ} = G_{ZIP} u_{bQ}, \quad \text{(A7)}$$

$$i_{QD} = -B_{ZIP} u_{bQ}, \quad i_{QQ} = B_{ZIP} u_{bQ}. \quad \text{(A8)}$$

REFERENCES

[1] Z. Shuai, Y. Sun, Z. J. Shen, W. Tian, C. Tu, and Y. Li *et al.*, "Microgrid stability: classification and a review," *Renewable & Sustainable Energy Reviews*, 58, 167-179, 2016.

[2] F. Tang, J. M. Guerrero, J. C. Vasquez, D. Wu, and L. Meng, "Distributed active synchronization strategy for microgrid seamless reconnection to the grid under unbalance and harmonic distortion," *IEEE Trans. Smart Grid*, vol. 6, no. 6, pp. 2757–2769, 2015.

[3] Z. Shuai, W. Huang, C. Shen, J. Ge, and J. Shen, "Characteristics and Restraining Method of Fast Transient Inrush Fault Currents in Synchronverters," *IEEE Trans. Ind. Electron.*, vol. 64, no. 9, pp. 7487-7497, Sept. 2017.

[4] Z. Shuai, C. Shen, X. Yin, X. Liu, and J. Shen, "Fault Analysis of Inverter-Interfaced Distributed Generators with Different Control Schemes," *IEEE Trans. Power Deliv.*, vol. 33, no. 3, pp. 1223-1235, Jun. 2018.

[5] M. Hamzeh, S. Emamian, H. Karimi and J. Mahseredjian, "Robust Control of an Islanded Microgrid Under Unbalanced and Nonlinear Load Conditions," *IEEE Journal of Emerging and Selected Topics in Power Electronics*, vol. 4, no. 2, pp. 512-520, June 2016.

[6] N. Pogaku, M. Prodanovic, and T. C. Green, "Modeling, Analysis and Testing of Autonomous Operation of an Inverter-Based Microgrid," *IEEE Trans. Power Electron.*, vol. 22, no. 2, pp. 613-625, March 2007.

[7] J. C. Vasquez, J. M. Guerrero, M. Savaghebi, J. Eloy-Garcia, and R. Teodorescu, "Modeling, analysis, and design of stationary-reference-frame droop-controlled parallel three-phase voltage source inverters," *IEEE Trans. Ind. Electron.*, vol. 60, no. 4, pp. 1271–1280, 2013.

[8] S. Leitner, M. Yazdanian, A. Mehrizi-Sani, and A. Muetze, "Small-Signal Stability Analysis of an Inverter-Based Microgrid with Internal Model–Based Controllers," *IEEE Trans. Smart Grid*, vol. 9, no. 5, pp. 5393-5402, Sept. 2018.

[9] X. Tang, W. Deng, and Z. Qi, "Investigation of the Dynamic Stability of Microgrid," *IEEE Trans. Power Syst.*, vol. 29, no. 2, pp. 698-706, March 2014.

[10] J. Alipoor, Y. Miura, and T. Ise, "Stability Assessment and Optimization Methods for Microgrid with Multiple VSG Units," *IEEE Trans. Smart Grid*, vol. 9, no. 2, pp. 1462-1471, March 2018.

[11] Y. Wang, X. Wang, F. Blaabjerg, and Z. Chen, "Harmonic Instability Assessment Using State-Space Modeling and Participation Analysis in Inverter-Fed Power Systems," *IEEE Trans. Ind. Electron.*, vol. 64, no. 1, pp. 806-816, Jan. 2017.

[12] M. Rasheduzzaman, J. A. Mueller, and J. W. Kimball, "An Accurate Small-Signal Model of Inverter- Dominated Islanded Microgrids Using dq Reference Frame," *IEEE J. Emerg. Sel. Top. Power Electron.*, vol. 2, no. 4, pp. 1070-1080, Dec. 2014.

[13] A. Aderibole, H. H. Zeineldin, and M. Al Hosani, "A Critical Assessment of Oscillatory Modes in Multi-Microgrids Comprising of Synchronous and Inverter Based Distributed Generation," *IEEE Trans. Smart Grid*, DOI: 10.1109/TSG.2018.2824330

[14] H. Khalil, Nonlinear Systems, Upper Saddle River, NJ, USA: PrenticeHall, 2002.

[15] M. Huang, Y. Peng, C. K. Tse, Y. Liu, J. Sun, and X. Zha, "Bifurcation and Large-Signal Stability Analysis of Three-Phase Voltage Source Converter Under Grid Voltage Dips," *IEEE Trans. Power Electron*, vol. 32, no. 11, pp. 8868-8879, Nov. 2017.

[16] M. Huang, H. Ji, J. Sun, L. Wei, and X. Zha, "Bifurcation-Based Stability Analysis of Photovoltaic-Battery Hybrid Power System," *IEEE J. Emerg. Sel. Top. Power Electron.*, vol. 5, no. 3, pp. 1055-1067, Sept. 2017.

[17] X. Wu, C. Shen, M. Zhao, Z. Wang and X. Huang, "Small signal security region of droop coefficients in autonomous microgrids," *2014 IEEE PES General Meeting | Conference & Exposition*, National Harbor, MD, 2014, pp. 1-5.

[18] Z. Shuai, Y. Hu, Y. Peng, C. Tu, and Z. J. Shen, "Dynamic Stability Analysis of Synchronverter-dominated Microgrid Based on Bifurcation Theory," *IEEE Trans. Ind. Electron.*, vol. 64, no. 9, pp. 7467-7477, Sept. 2017.

[19] E. Lenz Cesar, D. J. Pagano, and J. Pou, "Bifurcation Analysis of Parallel-Connected Voltage-Source Inverters with Constant Power Loads," *IEEE Trans. Smart Grid*, vol. 9, no. 6, pp. 5482-5493, Nov. 2018.

[20] G. Diaz, C. Gonzalez-Moran, J. Gomez-Aleixandre, and A. Diez, "Composite Loads in Stand-Alone Inverter-Based Microgrids -Modeling Procedure and Effects on Load Margin," *IEEE Trans. Power Syst.*, vol. 25, no. 2, pp. 894-905, May 2010.

[21] P. Vorobev, P. H. Huang, M. Al Hosani, J. L. Kirtley and K. Turitsyn, "High-Fidelity Model Order Reduction for Microgrids Stability Assessment," *IEEE Trans. Power Syst.*, vol. 33, no. 1, pp. 874-887, Jan. 2018.

[22] I. P. NIKOLAKAKOS, H. H. Zeineldin, M. S. El Moursi, and J. L. Kirtley, "Reduced-Order Model for Inter-Inverter Oscillations in Islanded Droop-Controlled Microgrids," *IEEE Trans. Smart Grid*, vol. 9, no. 5, pp. 4953-4963, Sept. 2018.

[23] M. Rasheduzzaman, J. A. Mueller, and J. W. Kimball, "Reduced-Order Small-Signal Model of Microgrid Systems," *IEEE Trans. Sustain. Energy*, vol. 6, no. 4, pp. 1292-1305, Oct. 2015.

[24] V. Mariani, F. Vasca, J. C. Vásquez, and J. M. Guerrero, "Model Order Reductions for Stability Analysis of Islanded Microgrids With Droop Control," *IEEE Trans. Ind. Electron.*, vol. 62, no. 7, pp. 4344-4354, July 2015.

[25] I. P. Nikolakakos, H. H. Zeineldin, M. S. El-Moursi, and N. D. Hatziargyriou, "Stability Evaluation of Interconnected Multi-Inverter Microgrids Through Critical Clusters," *IEEE Trans. Power Syst.*, vol. 31, no. 4, pp. 3060–3072, 2016.

[26] Z. Shuai, Y. Peng, X. Liu, Z. Li, J. M. Guerrero, and Z. J. Shen, "Dynamic Equivalent Modeling for Multi-Microgrid Based on Structure Preservation Method," *IEEE Trans. Smart Grid*, DOI: 10.1109/ TSG.2018.2844107.

[27] Y. Peng, Z. Shuai, J. Shen, J. Wang, C. Tu, and Y. Cheng, "Reduced order modeling method of inverter-based microgrid for stability analysis," *2017 IEEE Applied Power Electronics Conference and Exposition (APEC)*, Tampa, FL, 2017, pp. 3470-3474.

[28] A. Dhooge, W. Govaerts, and Y. A. Kuznetsov, Matcont: A Matlab package for numerical bifurcation analysis of ODEs, 2003. [Online]. Available: http://sourceforge.net/projects/matcont.

[29] J. He and Y. W. Li, "Analysis, design, and implementation of virtual impedance for power electronics interfaced distributed generation," *IEEE Trans. Ind. Appl.*, vol. 47, no. 6, pp. 2525–2538, 2011.

[30] J. Jeon, J. Kim, H. Kim, S. Kim, C. Cho, and J. Kim *et al.*, "Development of Hardware In-the-Loop Simulation System for Testing Operation and Control Functions of Microgrid," *IEEE Trans. Power Electron*, vol. 25, no. 12, pp. 2919-2929, Dec. 2010.

Zhikang Shuai (S'09-M'10-SM'17) received the B.S. and Ph.D. degree from the College of Electrical and Information Engineering, Hunan University, Changsha, China, in 2005 and 2011, respectively, all in electrical engineering. He was at Hunan University, as an Assistant Professor between 2009 and 2012, an Associate Professor in 2013, and a Professor in 2014. His research interests include power quality control, power electronics, and microgrid stability analysis and control. Dr. Shuai is the Associate Editor of IEEE Journal of Emerging and Selected Topics in Power Electronics, CSEE Journal of Power and Energy Systems, Chinese Journal of Electrical Engineering. He received the 2010 National Scientific and Technological Awards of China, the 2012 Hunan Technological Invention Awards of China, and the 2007 Scientific and Technological Awards from the National Mechanical Industry Association of China.

This article has been accepted for publication in a future issue of this journal, but has not been fully edited. Content may change prior to final publication. Citation information: DOI 10.1109/TSG.2019.2907600, IEEE Transactions on Smart Grid

Yelun Peng received the B.S. degree in electrical and information engineering from Changsha University of Science and Technology, Changsha, China, in 2013. He is currently pursuing the Ph.D. degree in electrical engineering at the college of electrical and information engineering from Hunan University, Changsha. In 2017, he was a guest Ph.D. student at the Department of Energy Technology, Aalborg University, Denmark. His research interests include modeling and stability analysis for the AC microgrid system.

Xuan Liu (M'14) received the B.S. and M.S degrees from Sichuan University, China, in 2008 and 2011, and the Ph.D. degree from the Illinois Institute of Technology (IIT), Chicago, in 2015, all in electrical engineering. He is currently a Professor in the College of Electrical and Information Engineering at Hunan University, China. His research interests include smart grid security, operation and economics of power systems.

Zuyi Li (SM'09) received the B.S. and M.S. degrees from Shanghai Jiaotong University, Shanghai, China, in 1995 and 1998, respectively, and the Ph.D. degree from the Illinois Institute of Technology (IIT), Chicago, in 2002, all in electrical engineering. Presently, he is a Professor in the Electrical and Computer Engineering Department at IIT. His research interests include economic and secure operation of electric power systems, cyber security in smart grid, renewable energy integration, electric demand management of data centers, and power system protection.

Josep M. Guerrero (S'01-M'04-SM'08-FM'15) received the B.S. degree in telecommunications engineering, the M.S. degree in electronics engineering, and the Ph.D. degree in power electronics from the Technical University of Catalonia, Barcelona, in 1997, 2000 and 2003, respectively. Since 2011, he has been a Full Professor with the Department of Energy Technology, Aalborg University, Denmark, where he is responsible for the Microgrid Research Program (www.microgrids.et.aau.dk). From 2012 he is a guest Professor at the Chinese Academy of Science and the Nanjing University of Aeronautics and Astronautics; from 2014 he is chair Professor in Shandong University; from 2015 he is a distinguished guest Professor in Hunan University; and from 2016 he is a visiting professor fellow at Aston University, UK, and a guest Professor at the Nanjing University of Posts and Telecommunications. His research interests is oriented to different microgrid aspects, including power electronics, distributed energy-storage systems, hierarchical and cooperative control, energy management systems, smart metering and the internet of things for AC/DC microgrid clusters and islanded minigrids; recently specially focused on maritime microgrids for electrical ships, vessels, ferries and seaports.

Z. John Shen (S'89-M'94-SM'01-F'11) received BS from Tsinghua University, China, in 1987, and M.S. and Ph.D. degrees from Rensselaer Polytechnic Institute, Troy, NY, in 1991 and 1994, respectively, all in electrical engineering.

He was on faculty of the University of Michigan-Dearborn between 1999 and 2004, and the University of Central Florida between 2004 and 2012. He joined the Illinois Institute of Technology in 2013 as the Grainger Chair Professor in Electrical and Power Engineering. He has also held a courtesy professorship with Hunan University, China since 2007; and with Zhejiang University, China since 2013. His research interests include power electronics, and power semiconductor devices, etc.

Dr. Shen has been an active volunteer in the IEEE Power Electronics Society, and has served as VP of Products 2009-2012, Associate Editor and Guest Editor in Chief of IEEE Transactions on Power Electronics, technical program chair and general chair of several major IEEE conferences.